

Surface Reaction Kinetics of $\text{Ga}_{1-x}\text{In}_x\text{P}$ Growth During Pulsed Chemical Beam Epitaxy

N. Dietz^{1,*}, S. C. Beeler², J. W. Schmidt², and H. T. Tran²

¹ *Department of Physics and Astronomy, University Plaza, Georgia State University, Atlanta, GA 30303-3083*

² *Center for Research in Scientific Computation and Department of Mathematics, Box 8205, North Carolina State University, Raleigh, NC 27695-8205*

Abstract

The understanding of thin film growth processes and their control requires the development of surface-sensitive real-time optical characterization techniques that are able to provide insight into the surface reaction kinetics during an organometallic deposition process. These insights will allow us to move the control point closer to the point where the growth occurs, which in a chemical beam epitaxy process is a surface reaction layer (SRL), built up of physisorbed and chemisorbed precursor fragments between the ambient and film interface. This contribution presents results on parameter estimations of rate constants and optical response factors in a reduced order surface kinetics (ROSK) model, which has been developed to describe the decomposition and growth kinetics of the involved organometallic precursors and their incorporation in the film deposition. As a real time characterization technique, we applied p -polarized reflectance spectroscopy (PRS) during low temperature growth of epitaxial $\text{Ga}_{1-x}\text{In}_x\text{P}$ heterostructures on Si(001) substrates by pulsed chemical beam epitaxy (PCBE). The high surface sensitivity of PRS allows us to follow alterations in composition and thickness of the SRL as they are encountered during periodic precursor supply. The linkage of the PRS response to the ROSK model provides the base for the parameter estimation, giving insights into the organometallic precursor decomposition and growth kinetics.

*Corresponding author. Tel.: (404)463-9617; Fax: (404)651-1427; E-mail: ndietz@gsu.edu

Report Documentation Page			Form Approved OMB No. 0704-0188		
Public reporting burden for the collection of information is estimated to average 1 hour per response, including the time for reviewing instructions, searching existing data sources, gathering and maintaining the data needed, and completing and reviewing the collection of information. Send comments regarding this burden estimate or any other aspect of this collection of information, including suggestions for reducing this burden, to Washington Headquarters Services, Directorate for Information Operations and Reports, 1215 Jefferson Davis Highway, Suite 1204, Arlington VA 22202-4302. Respondents should be aware that notwithstanding any other provision of law, no person shall be subject to a penalty for failing to comply with a collection of information if it does not display a currently valid OMB control number.					
1. REPORT DATE 2000		2. REPORT TYPE		3. DATES COVERED 00-00-2000 to 00-00-2000	
4. TITLE AND SUBTITLE Surface Reaction Kinetics of Ga_{1-x}In_xP Growth During Pulsed Chemical Beam Epitaxy				5a. CONTRACT NUMBER	
				5b. GRANT NUMBER	
				5c. PROGRAM ELEMENT NUMBER	
6. AUTHOR(S)				5d. PROJECT NUMBER	
				5e. TASK NUMBER	
				5f. WORK UNIT NUMBER	
7. PERFORMING ORGANIZATION NAME(S) AND ADDRESS(ES) North Carolina State University, Center for Research in Scientific Computation, Raleigh, NC, 27695-8205				8. PERFORMING ORGANIZATION REPORT NUMBER	
9. SPONSORING/MONITORING AGENCY NAME(S) AND ADDRESS(ES)				10. SPONSOR/MONITOR'S ACRONYM(S)	
				11. SPONSOR/MONITOR'S REPORT NUMBER(S)	
12. DISTRIBUTION/AVAILABILITY STATEMENT Approved for public release; distribution unlimited					
13. SUPPLEMENTARY NOTES The original document contains color images.					
14. ABSTRACT see report					
15. SUBJECT TERMS					
16. SECURITY CLASSIFICATION OF:			17. LIMITATION OF ABSTRACT	18. NUMBER OF PAGES 16	19a. NAME OF RESPONSIBLE PERSON
a. REPORT unclassified	b. ABSTRACT unclassified	c. THIS PAGE unclassified			

1. Introduction

The engineering of advanced optoelectric devices, microelectronic circuits, and integrated optical circuits requires precise control of lateral dimensions and thicknesses of device features and perfection of heterostructures. Low pressure deposition methods, such as chemical beam epitaxy (CBE) and plasma enhanced chemical vapor deposition, play an important role in the manufacturing of nanostructure devices and advanced ultra-large scale integration (ULSI) processing, respectively. Some areas of interest include improved densities of integrated electronic devices and methods of improving the control of epitaxial deposition to realize these devices. Key targets in III-V compound/silicon heterostructures are the control and understanding of defect formation and the interactions and propagations of defects during later stages of compound heteroepitaxy growth. To understand the properties of defects in the epitaxial film, we must understand the kinetics of thin film growth.

Understanding and controlling thin film growth has been a slow process because little is known about chemical reaction properties and reaction kinetics parameters during the decomposition process of metalorganic precursors. In the film deposition process, the film surface plays a major role in the growth process as the addition of new reactants can significantly modify the growth chemistries [1, 2]. This characteristic of thin film growth chemistry during chemical deposition combined with the demand for stringent thickness and composition control in advanced optoelectronic integrated circuits has led to the development of surface sensitive real-time optical sensors [3, 4] that are able to move the monitoring and control point closer to the point where growth occurs, which in a chemical beam epitaxy process is the SRL. The SRL is built up of physisorbed and chemisorbed precursor fragments between the ambient and film interface.

Applying optical probe techniques to real-time characterization of thin film growth includes the challenge of relating surface chemistry processes that drive the growth process to growth and film properties, such as composition, instantaneous growth rate, or structural quality. Most characterization techniques take advantage of the numerous probes available to provide a detailed assessment of the ambient by accurately measuring ambient process parameters, but they are limited in their ability to deal with complex surface chemistry processes. For example, during heteroepitaxial GaP/Ga_{1-x}In_xP growth on Si under pulsed CBE (PCBE) conditions, the surface is exposed to a periodic supply of metalorganic precursors, which results in an SRL with periodically altered thickness and composition. The measurement technique of *p*-polarized reflectance spectroscopy (PRS) [5, 6, 7], which has demonstrated high sensitivity towards surface reaction processes in the context of real-time monitoring of PCBE, allows us to undertake the desired characterization and control of thin film deposition.

We start in Section 2 with a brief background on the experimental growth and monitoring conditions and show results obtained by PRS during real-time characterization of heteroepitaxial growth of Ga_{1-x}In_xP on Si substrates. In Section 3, we introduce the model used to simulate the PRS measurements. We also describe the link of the PR response to the simulation parameters accessible through the reduced order surface kinetics (ROSK) model, which has been developed to describe the decomposition and growth kinetics of the involved organometallic precursors [4, 8]. The process of identifying these parameters is explained in Section 4. Section 5 analyzes the results of the parameter identification, allowing us to establish and validate surface reaction kinetics parameters, while advancing our understanding of fundamental chemistry processes in thin film growth using organometallic precursors. We finish with our concluding remarks in Section 6.

2. Experimental Setup and Results

For monitoring both the bulk and surface properties during heteroepitaxial $\text{Ga}_{1-x}\text{In}_x\text{P}$ growth on Si, PRS has been integrated into the pulsed chemical beam epitaxy system that is schematically shown in Figure 1. In PCBE, the surface of the substrate is exposed to pulsed ballistic beams of

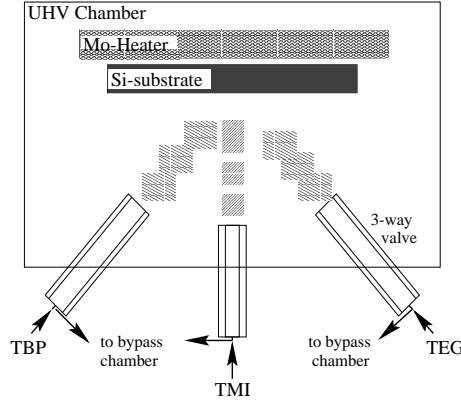


Figure 1: Setup of PCBE system for III-V compound semiconductor growth.

TBP $[(\text{C}_4\text{H}_9)\text{PH}_2]$, TEG $[\text{Ga}(\text{C}_2\text{H}_5)_3]$, and TMI $[\text{In}(\text{CH}_3)_3]$ at typically 350-450° C to accomplish nucleation and overgrowth of the silicon by an epitaxial GaP/ $\text{Ga}_{1-x}\text{In}_x\text{P}$ film. For PRS and laser light scattering (LLS), we employ *p*-polarized light beams with wavelengths $\lambda = 632.8$ nm and 650 nm at two angles of incidence (PR70: $\Phi_1 = 71.5^\circ$ and PR75: $\Phi_1 = 75.8^\circ$). Further information on the experimental conditions is provided in previous publications [4]-[9].

Each growth run is started with a preconditioning period, where the substrate temperature is raised to the growth temperature and the PR signals change according to the temperature dependency of the substrate dielectric function. We use the PR signals to verify independent temperature measurements and calibrate the actual surface temperature. A constant flow of Palladium purified H_2 (10 sccm) is introduced to the growth chamber during the preconditioning and growth periods. The background pressure is 10^{-9} torr and the pressure during growth is in the range of 10^{-3} - 10^{-4} torr.

The growth sequence starts typically after 1200 s of preconditioning with 250 cycles of GaP growth to aid in lattice matched $\text{Ga}_{1-x}\text{In}_x\text{P}$ growth on a Si(001) substrate. After the deposition of a GaP layer, the transition to $\text{Ga}_{1-x}\text{In}_x\text{P}$ was made in one of three ways. The first transition was an abrupt change to the desired TMI:TEG flow ratio. The other two transitions are graded changes, done linearly either manually or under computer control, from a TMI:TEG flow ratio of 0 to the desired flow ratio (0-1). This flow ratio relates to the composition, x , of $\text{Ga}_{1-x}\text{In}_x\text{P}$ as discussed in Section 3.

Figure 2 shows the PR and LLS signals during heteroepitaxial growth of $\text{Ga}_{1-x}\text{In}_x\text{P}$ on Si(001). After initiating growth, the minima and maxima observed in the PR signals are due to the interference phenomena as the film grows. Note that the maxima and minima of the two signals are phase shifted, due to the fact that one angle of incidence (PR75) is above, and the other (PR70) below the pseudo-Brewster angle of the growing film. Superimposed on the interference fringes is a fine structure, which is due to the periodically modulated composition and thickness of the SRL.

For the surface reaction kinetics analysis and the validation of performed simulations using the

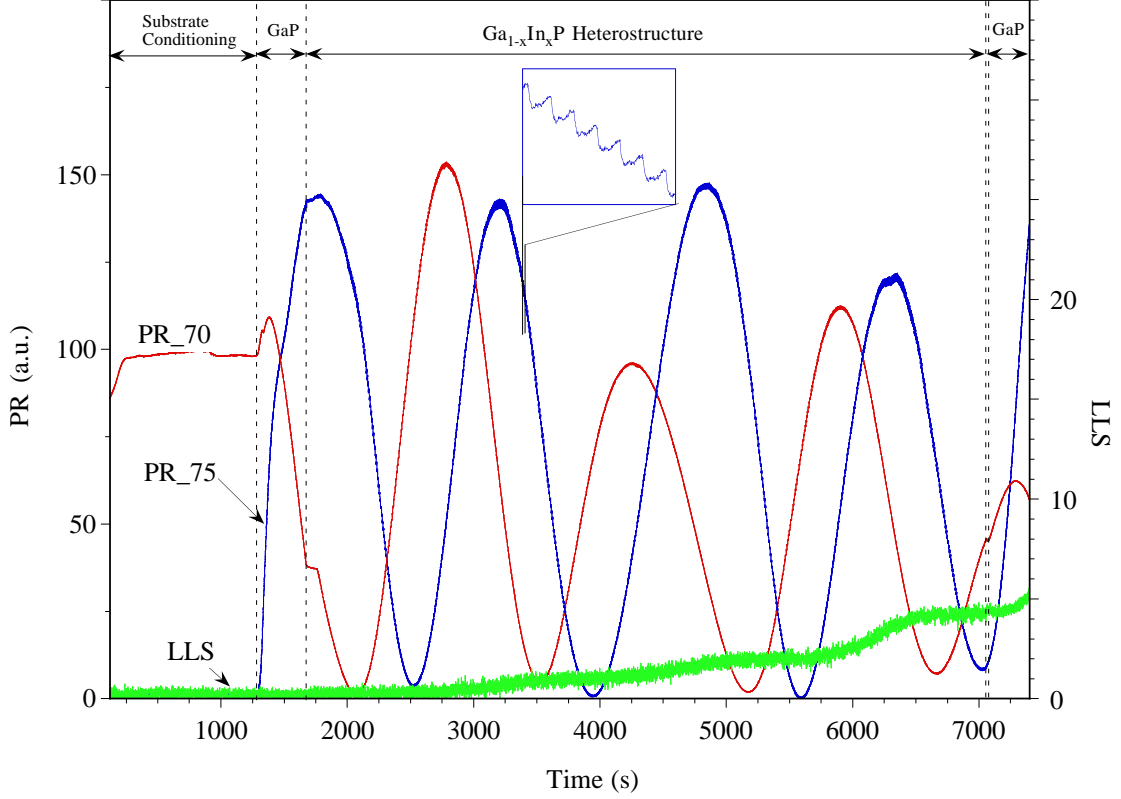


Figure 2: Monitoring of heteroepitaxial $\text{Ga}_{1-x}\text{In}_x\text{P}$ growth under PCBE by PRS and LLS. The inset enlargement shows the PR response to a periodically modulated SRL composition and thickness during pulsed precursor supply.

ROSK model presented in Section 3, we varied one experimental parameter, the TMI flow rate. Each growth condition was set to the specified TMI:TEG flow ratio and monitored for at least $1\frac{1}{2}$ interference oscillations in order to get stable steady-state growth and gather sufficient information to analyze and simulate the growth process.

The correlation of the fine structure evolution with the pulsing sequence of the precursor supply is depicted in Figure 3. In Figure 3, the PR response is taken during steady-state growth on a rising flank of an interference oscillation using a pulse cycle sequence of 6 s, a TBP pulse from 0.0-0.8 s and 3.0-3.8 s, a TEG pulse from 1.5-1.8 s, a TMI pulse from 4.5-4.8 s, and a continuous hydrogen flow during the complete sequence. In this set of experiments, the flow rates and pulse durations of TBP (1.0 sccm for 800 ms) and TEG (0.054 sccm for 300 ms) were kept constant, as was the pulse duration of TMI (300 ms). The flow rate for TMI was varied from 0.014 to 0.068 sccm to produce the desired TMI:TEG flow ratios and compositions, x , of $\text{Ga}_{1-x}\text{In}_x\text{P}$. As the TMI:TEG flow ratio increases, the magnitude of the fine structure increases according to a larger quantity of TMI constituents in the SRL. The results are discussed in more detail in Section 5, which includes comparisons with the results of simulations.

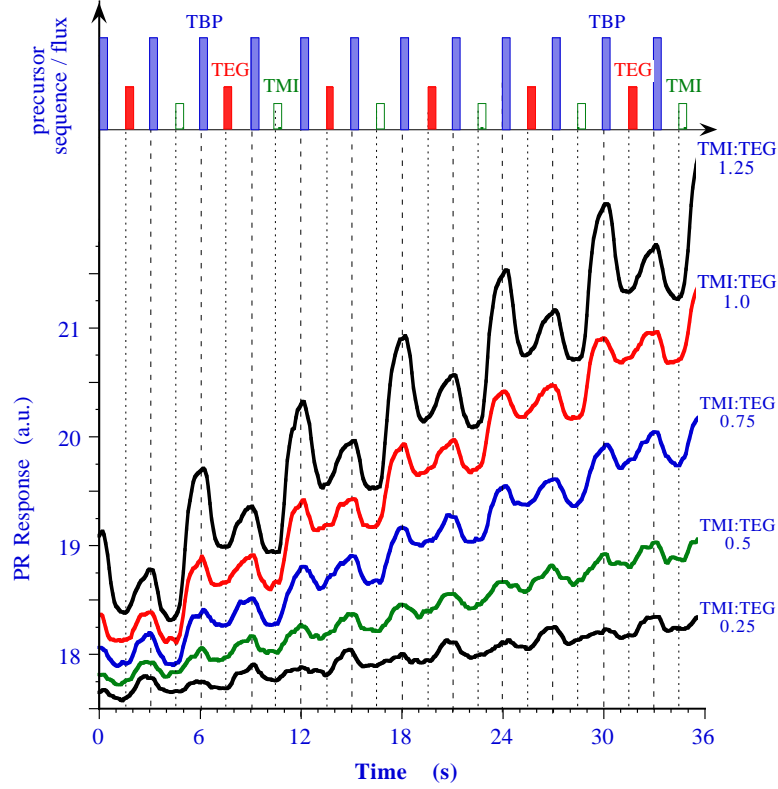


Figure 3: A comparison of PR75 response to periodically modulated TBP, TEG, and TMI precursor pulses for different TMI:TEG flow ratios (0.25–0.5–0.75–1.0–1.25) at the rising flank of an interference oscillation.

3. Modeling of PRS Results

To model the optical responses, the growing heteroepitaxial film is approximated by a four layer model consisting of: (1) ambient – (2) surface reaction layer (SRL) – (3) film – (4) substrate. We consider here $\text{Ga}_{1-x}\text{In}_x\text{P}$ on a Si/GaP virtual substrate. The complex reflectivity coefficient for p -polarized incident light, given a four-layer stack, is given by the formula

$$r_p = \frac{r_{12}(1 + r_{23}r_{34}e^{-2i\beta_3}) + (r_{23} + r_{34}e^{-2i\beta_3})e^{-2i\beta_2}}{(1 + r_{23}r_{34}e^{-2i\beta_3}) + r_{12}(r_{23} + r_{34}e^{-2i\beta_3})e^{-2i\beta_2}}, \quad (1)$$

where the Fresnel coefficients $r_{k(k+1)}$ ($k = 1, 2, 3$) for each interface are given by

$$r_{k(k+1)} = \frac{\epsilon_{k+1}\sqrt{\epsilon_k - \epsilon_1\sin^2\Phi_1} - \epsilon_k\sqrt{\epsilon_{k+1} - \epsilon_1\sin^2\Phi_1}}{\epsilon_{k+1}\sqrt{\epsilon_k - \epsilon_1\sin^2\Phi_1} + \epsilon_k\sqrt{\epsilon_{k+1} - \epsilon_1\sin^2\Phi_1}}, \quad (2)$$

and the phase angles β_k for the SRL ($k = 2$) and the growing film epilayer ($k = 3$) are given by

$$\beta_k = \frac{2\pi}{\lambda}d_k\sqrt{\epsilon_k - \epsilon_1\sin^2\Phi_1}. \quad (3)$$

In equations (1)-(3), the reflectivity coefficient r_p is a function of d_2 and d_3 (the thickness of the SRL and film respectively), ϵ_1 , ϵ_2 , ϵ_3 , and ϵ_4 (the complex dielectric functions of the ambient, SRL, film, and substrate respectively), Φ_1 (the angle of incidence), and λ (the wavelength of the impinging laser light). For additional information, we refer the reader to [9].

The values of ϵ_1 , ϵ_3 , ϵ_4 , Φ_1 , and λ are all constant in time, but ϵ_2 , d_2 , and d_3 vary in time as the film grows and the SRL changes in composition and thickness. To understand how these values change, we need a representative model of the chemical kinetics of the SRL which approximates the pyrolysis of the source vapor molecules as described previously [10, 11, 12]. For TBP, TEG, and TMI as source vapors forming $\text{Ga}_{1-x}\text{In}_x\text{P}$, we employ a reduced order surface kinetics (ROSK) model [4, 8]. The ROSK model makes the following simplifying assumptions:

- TBP pyrolysis is approximated through one dominant reaction equation.
- TEG decomposition is simplified to two dominant reaction equations.
- The formation of GaP is combined into one dominant reaction equation.
- TMI decomposition is simplified to two dominant reaction equations.
- The formation of InP is combined into one dominant reaction equation.
- The process is driven by a periodic source vapor supply as described in Section 2.

Thus the kinetic model representing the SRL reactions can be represented by the following system of ordinary differential equations:

$$\frac{d}{dt}n_1(t) = S_1(t) - k_1n_1(t) - k_{\text{GaP}}n_1(t)n_3(t)\frac{1}{10^{-8}\text{mol}} - k_{\text{InP}}n_1(t)n_6(t)\frac{1}{10^{-8}\text{mol}} \quad (4)$$

$$\frac{d}{dt}n_2(t) = S_2(t) - k_{\text{dTEG}}n_2(t) - k_2n_2(t) \quad (5)$$

$$\frac{d}{dt}n_3(t) = k_2n_2(t) - k_3n_3(t) - k_{\text{GaP}}n_1(t)n_3(t)\frac{1}{10^{-8}\text{mol}} \quad (6)$$

$$\frac{d}{dt}n_4(t) = k_{\text{GaP}}n_1(t)n_3(t)\frac{1}{10^{-8}\text{mol}} \quad (7)$$

$$\frac{d}{dt}n_5(t) = S_3(t) - k_{\text{dTMI}}n_5(t) - k_5n_5(t) \quad (8)$$

$$\frac{d}{dt}n_6(t) = k_5n_5(t) - k_6n_6(t) - k_{\text{InP}}n_1(t)n_6(t)\frac{1}{10^{-8}\text{mol}} \quad (9)$$

$$\frac{d}{dt}n_7(t) = k_{\text{InP}}n_1(t)n_6(t)\frac{1}{10^{-8}\text{mol}} \quad (10)$$

The units of each term of these equations is mol/s. The reaction constants, k_i , have units of s^{-1} , while the molar quantities, n_i , have units of mol. The state variables represent the number of moles of the various components of the SRL, such as n_1 for active surface phosphorus fragments. The intermediate gallium precursor fragments in the TEG decomposition, possibly diethylgallium (DEG), are represented by n_2 and the active gallium fragments are represented by n_3 . Similarly, the intermediate indium precursor fragments and the active indium fragments are represented by n_5 and n_6 respectively. In equation (4), the change in active surface phosphorus fragments is written as the sum of a source term S_1 , a desorption loss term $-k_1n_1$, and reaction terms representing the

formation of GaP and InP. Equation (5), which represents the defragmentation process of TEG, contains a source term S_2 , a desorption loss term, and a term of decomposition from the intermediate gallium precursor fragments to active surface gallium fragments. Equation (6), which represents the change active surface gallium fragments, has a term of creation from the intermediate gallium fragments, a desorption loss term, and a reaction term for the formation of GaP. Equation (8), which describes the defragmentation of TMI, contains a source term S_3 , a desorption loss term, and a term of decomposition from the intermediate indium precursor fragments to active surface indium fragments. Equation (9), which represents the change in active surface indium fragments, has a term of creation from the intermediate indium fragments, a desorption loss term, and a reaction term for the formation of InP. The variables n_4 and n_7 represent the number of moles of created GaP and InP, respectively, integrated in the deposited $\text{Ga}_{1-x}\text{In}_x\text{P}$ film layer. Equation (7) contains only a single reaction term for the formation of GaP from active surface Ga and P, and equation (10) contains only a single reaction term for the formation of InP from active surface In and P. These two equations also account for any surface activation processes.

The source terms in the differential equations are based on the source vapor pulses. These are modeled similarly to the GaP case [13], with the TBP source given by the expression

$$S_1(t) = \frac{P_1(t)\gamma\beta_{\text{TBP}}}{V_{\text{TBP}}}, \quad (11)$$

where $P_1(t)$ is the source vapor injection rate, V_{TBP} is the molar volume of TBP, and the constant β_{TBP} is the sticking coefficient of TBP. The geometrical parameter γ represents the amount of source vapors that actually hit the surface of the wafer, which is a constant value for a given reactor geometry. Similarly, the second and third source terms are modeled by

$$S_2(t) = \frac{P_2(t)\gamma\beta_{\text{TEG}}}{V_{\text{TEG}}}, \quad (12)$$

$$S_3(t) = \frac{P_3(t)\gamma\beta_{\text{TMI}}}{V_{\text{TMI}}}, \quad (13)$$

with corresponding $P_2(t)$, V_{TEG} , and β_{TEG} for the TEG pulse, and $P_3(t)$, V_{TMI} , and β_{TMI} for the TMI pulse. The same constant γ appears in all source terms. For each source term, we use a constant flow rate between start and stop times, and zero flow elsewhere. Due to the time needed for the source vapor gates to open and close and for the vapors to travel to the surface, there is a small time difference between the start (and stop) of the vapor pulse and the start (and stop) of the source vapor arrival at the surface. We account for this time difference with a parameter *delay*. With a source vapor pulse starting at t_{on} and stopping at t_{off} , the source vapors actually reach the surface starting at $t_{\text{on}} + \text{delay}$ and ending at $t_{\text{off}} + \text{delay}$. We estimated a delay of 0.27 s using the parameter estimation process as described in Section 4.

The system of differential equations (4)-(10), together with the source terms (11)-(13), and appropriate initial conditions, can be solved numerically for the number of moles n_1 , n_2 , n_3 , n_4 , n_5 , n_6 , and n_7 . From these solutions, the film and SRL thicknesses are obtained from the formulas [4]

$$d_3(t) = \frac{1}{A}[V_{\text{GaP}}n_4(t) + V_{\text{InP}}n_7(t)], \quad (14)$$

$$d_2(t) = \frac{\alpha_{\text{SRL}}}{A}[V_1n_1(t) + V_2n_2(t) + V_3n_3(t) + V_5n_5(t) + V_6n_6(t)], \quad (15)$$

where A is the surface area of the wafer, V_k are the molar volumes of the components n_k , and V_{GaP} and V_{InP} are the molar volumes of GaP and InP, respectively. Finally, α_{SRL} is an effective SRL

thickness parameter representing the percentage of the SRL that contributes to the optical response. The effective dielectric function of the SRL is expressed as the sum over all molar fractions x_i contributing to the SRL and is given by

$$\epsilon_2(t) = 1 + \sum_{i \neq 4,7} x_i(t) F_i \quad \text{and} \quad x_i(t) = \frac{n_i(t)}{\sum_k n_k(t)}, \quad (16)$$

which is derived from the Sellmeier equation [4, 14].

With the values of the temporal dependent parameters ϵ_2 , d_2 , and d_3 found by equations (14)-(16) and with the constant parameters ϵ_1 , ϵ_3 , ϵ_4 , Φ_1 , and λ , the reflectivity coefficient r_p can be calculated using equations (1)-(3). From r_p , we then find the value that is actually measured in the experiments by computing the reflectance $R_p = |r_p|^2$.

Finally, the composition, x , for the compound semiconductor $\text{Ga}_{1-x}\text{In}_x\text{P}$ is expressed as the averaged molar ratio of molar concentration over a cycle sequence [4]:

$$x = \frac{\int_{t=0 \text{ sec}}^{t=6 \text{ sec}} \frac{d}{dt} n_7 dt}{\int_{t=0 \text{ sec}}^{t=6 \text{ sec}} \left(\frac{d}{dt} n_4 + \frac{d}{dt} n_7 \right) dt}. \quad (17)$$

The instantaneous film growth rate, g_{fl} , is given by

$$g_{fl} = \frac{1}{A} \left[V_{\text{GaP}} \frac{d}{dt} n_4 + V_{\text{InP}} \frac{d}{dt} n_7 \right]. \quad (18)$$

In the equations described above, Φ_1 , λ , ϵ_1 , V_1 , V_2 , V_3 , V_5 , V_6 , V_{GaP} , V_{InP} , V_{TBP} , V_{TEG} , V_{TMI} , A , β_{TBP} , β_{TEG} , β_{TMI} , α_{SRL} , and all start/stop times and flow rates contributing to P_1 , P_2 , and P_3 are known quantities. The values of the dielectric functions ϵ_3 and ϵ_4 , the rate constants k_1 , k_2 , k_3 , k_5 , k_6 , k_{dTEG} , k_{dTMI} , k_{GaP} , and k_{InP} , the optical responses F_1 , F_2 , F_3 , F_5 , and F_6 , the geometrical parameter γ , and *delay* have to be determined. In the next section, an inverse least squares problem will be formulated to estimate these parameters. The comparison of the model using the estimated parameters with the experimental data will be done in Section 5.

4. Three Layer Problem and Setup of Parameter Identification

We formulate here an inverse least squares problem for identifying the unknown parameters in the model in Section 3. We want the set of parameters that results in the modeled reflectance most closely matching the experimental data. For this we look for the vector of parameters

$$\vec{q} = (F_1, F_2, F_3, F_5, F_6, k_1, k_{\text{dTEG}}, k_2, k_3, k_{\text{GaP}}, k_{\text{dTMI}}, k_5, k_6, k_{\text{InP}}, \gamma, \text{delay}) \quad (19)$$

that minimizes the cost function

$$J(\vec{q}) = \sqrt{\sum_i (R_{\text{exp}}(t_i) - R_{\text{calc}}(t_i, \vec{q}))^2}. \quad (20)$$

In this cost function, $R_{\text{exp}}(t_i)$ is the experimental reflectance data set at the measurement times t_i , and $R_{\text{calc}}(t_i, \vec{q}) = |r_p|^2$, where r_p is the complex reflectivity coefficient given by (1), is the simulated reflectance calculated at the same times using the parameter set \vec{q} .

Since larger numbers of parameters make the minimization process increasingly difficult, we do not include ϵ_3 and ϵ_4 in \vec{q} . We are able to remove these two parameters from our large parameter estimation problem by formulating a separate but simpler estimation problem. The simpler problem uses a three-layer stack as a model of the growing film by removing the SRL from consideration and leaving just the ambient, film, and substrate layers. This allows us to first study the properties of the film itself before later looking at the behavior in the SRL. The formula for calculating the reflectance for a three-layer stack is given by

$$r_{3,p} = \frac{r_{13} + r_{34}e^{-2i\beta_3}}{1 + r_{13}r_{34}e^{-2i\beta_3}}, \quad (21)$$

where r_{13} and r_{34} are Fresnel coefficients for the reflection from interfaces 1-3 and 3-4 (now that layer 2, the SRL, is removed), and the phase angle β_3 is for the film layer. These values are calculated by formulas analogous to (2) and (3).

To compare results from this formula with experimental results, we use a method described previously in our investigation with GaP formation [13]. At this point we focus on the large-amplitude interference oscillations, which have a periodicity of several hundreds of seconds and are formed by the film growth, and remove the small-amplitude fine structure oscillations that are modulated with the precursor injection. After extracting the experimental three-layer stack reflectance $R_{3,\text{exp}}$, we can identify the parameters ϵ_3 and ϵ_4 , as well as the average growth rate, \hat{g}_r , which is used to find the film thickness at times t_i , by comparing the calculated reflectance $R_{3,\text{calc}} = |r_{3,p}|^2$ from equation (21) to $R_{3,\text{exp}}$. This is done through an inverse least squares formulation by finding $\vec{r} = (\epsilon_3, \epsilon_4, \hat{g}_r)$ that minimizes the cost function

$$J(\vec{r}) = \sqrt{\sum_i (R_{3,\text{exp}}(t_i) - R_{3,\text{calc}}(t_i, \vec{r}))^2}. \quad (22)$$

The results of the three-layer curve fitting provide us with the average growth rate, \hat{g}_r , and the film dielectric, ϵ_3 , for each TMI:TEG flow ratio. The substrate dielectric, ϵ_4 , is also found, but is not flow ratio specific since it takes into account the initial GaP layer and the abrupt or graded change in precursor pulse flow to the desired TMI:TEG flow ratio of $\text{Ga}_{1-x}\text{In}_x\text{P}$ film growth. Specific parameter estimates for different flow ratios are presented in Table 1.

TMI:TEG flow ratio	0.25	0.5	0.75	1.0	1.25
\hat{g}_r (Å/s)	0.31	0.41	0.61	0.80	0.93
ϵ_3	10.56-1.30i	10.94-1.48i	10.53-1.08i	10.15-1.50i	11.28-0.65i

Table 1: Average values of flow ratio specific three-layer model parameters

Once we have determined the values of ϵ_3 , ϵ_4 , and \hat{g}_r , these parameters are used to solve the four-layer stack parameter identification problem, which finds the unknown parameters $F_1, F_2, F_3, F_5, F_6, k_1, k_{\text{dTEG}}, k_2, k_3, k_{\text{GaP}}, k_{\text{dTMI}}, k_5, k_6, k_{\text{InP}}, \gamma$, and *delay*.

5. $\text{Ga}_{1-x}\text{In}_x\text{P}$ Growth Kinetics Analysis

We compare measurements taken with various TMI:TEG flow ratios while all other conditions are fixed so that we may determine the dielectric function (ϵ_2) corresponding to a given composition, x ,

of $\text{Ga}_{1-x}\text{In}_x\text{P}$. In addition, varying the TMI:TEG flow ratio reveals several important characteristics in the fine structure. We will explain these features and show how the mathematical model of the growth process, using the reduced order surface kinetics model described in Section 3, captures these phenomena.

Looking at the fine structure in the PR 75 data, the most noticeable change that occurs with the TMI:TEG flow ratio variation is the increasing of the fine structure amplitude as TMI:TEG flow ratio increases, as illustrated in Figure 4. The regions near the TBP pulse exhibit an upward slope in

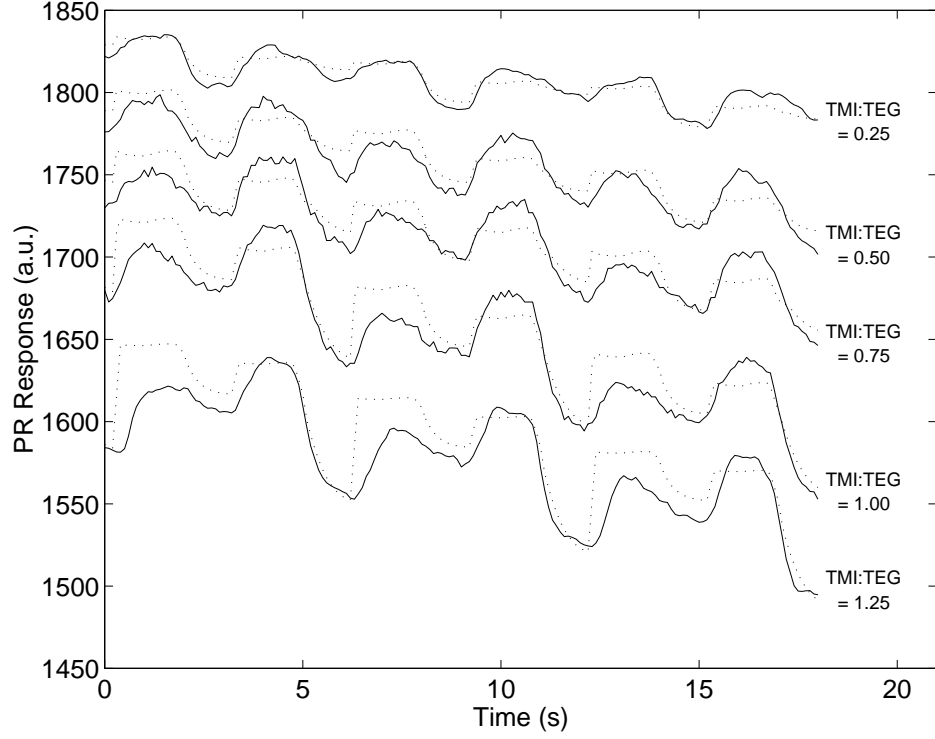


Figure 4: Experimental and simulated PR75 responses for various TMI:TEG flow rates under steady-state growth conditions.

the fine structure, while the regions near the TEG pulse exhibit a downward slope, as was described in work with GaP [13]. The upward slope in the optical response is due to the source TBP exposure, the defragmentation, and the generation of active phosphorus on the surface, while the downward slope is due to the source TEG exposure, the defragmentation, and the active gallium generation on the surface. The regions in the optical response fine structure related to a TMI exposure exhibit a downward slope, much like the TEG exposure, except that the deflection is on a much larger scale for the larger TMI flow rates.

In Figure 4 we can also examine the changes in the simulated and experimental data as we varied the TMI:TEG flow ratio. Here we see that the amplitude of the fine structure increases, especially after the TMI pulse, as we increase the flow ratio. In addition, the steeper slope in the interference fringes is related to the increase in the overall growth rate due to the greater TMI flow. Both the experimental and simulated data sets exhibit these characteristics and the results agree with each other very well.

One larger-scale feature observed in the reflectance data is change in the average film growth rate for the various TMI:TEG flow ratios. The frequency of the large-scale interference fringes is also related to the TMI:TEG flow ratio and the average film growth rate. Equations (2), (3), and (21) illustrate that a larger growth rate corresponds to a more quickly increasing d_3 and β_3 , which increases the frequency of the interference fringes.

The other large-scale characteristic feature of the data set is the position of (or the lack of) turning points in the fine structure, which can be depicted in the first derivative of the reflectance data, as shown in Figure 5. The turning point positions are characterized by the PR measurements

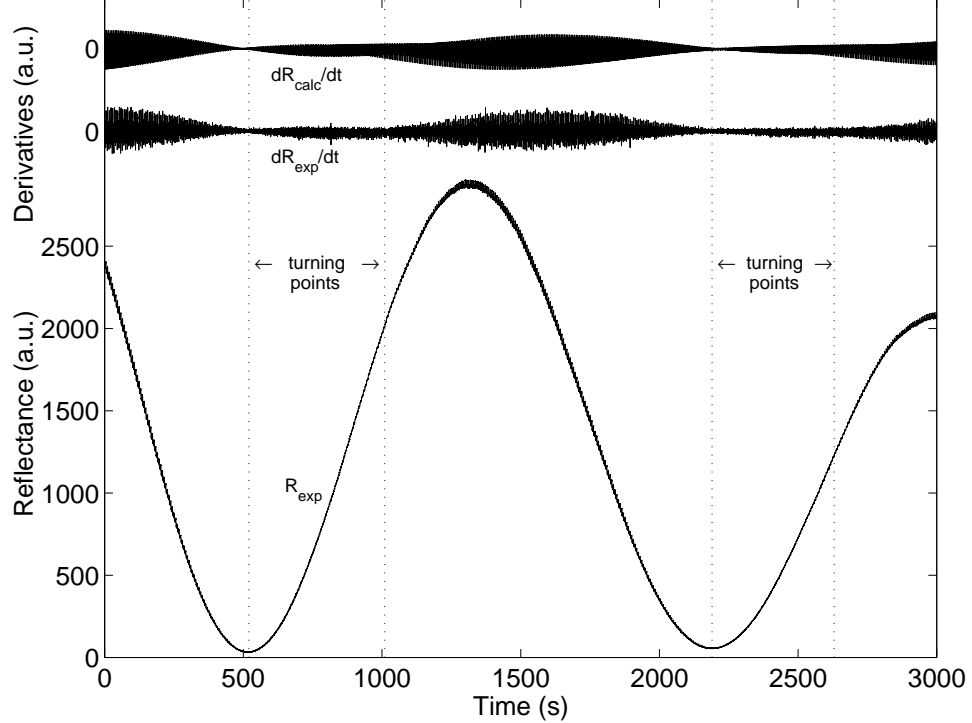


Figure 5: The first derivatives of the simulated and experimental reflectance data, shown with the experimental data set.

through the places where the amplitude of the reflectance derivative is minimized. There will either be pairs of turning points for each interference oscillation, as the fine structure switches sign, or a single minimum in the case that there is no sign change. Since the turning point positions are functions of the SRL dielectric properties, the good match between the derivatives in Figure 5 implies that the SRL dielectric properties have been well represented by the model.

The steps in the generation of the set of simulated data for flow ratio 0.75 presented in Figure 4 are shown in detail in Figure 6. The five SRL components are the result of the source pulses and the ROSK simulations. Once we have the SRL components, we find the SRL thickness and dielectric function. These values then are used to calculate the reflectance. Figure 6 shows how the exposure of the growth surface to TBP changes the SRL and with it the optical response, causing an upward slope in the fine structure. Similarly the TEG and TMI exposures cause changes in the SRL which result in downward slopes in the optical response. The good fit of the simulated fine structure to the

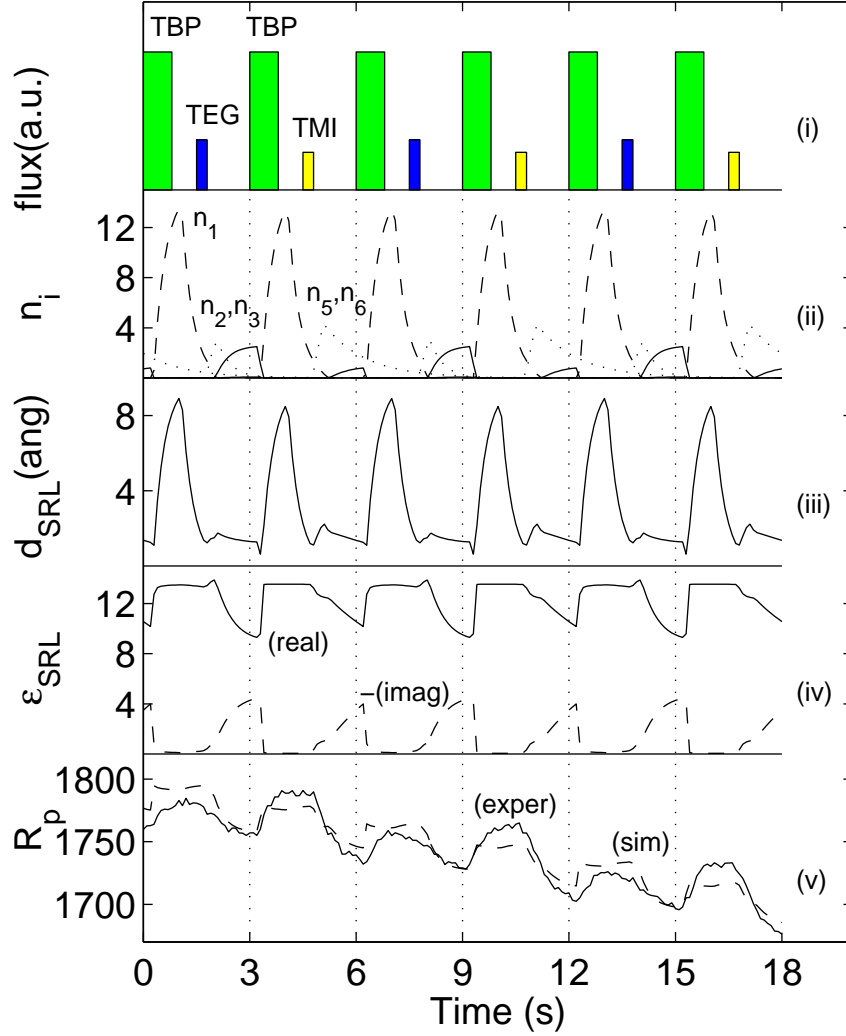


Figure 6: The steps in the generation of a set of simulated data are each represented by their contributing numerical solutions. In order from top to bottom: (i) the flux of precursor pulses, (ii) the molar quantities, $n_i(t)$, (iii) the SRL thickness, $d_2(t)$, (iv) the SRL dielectric function, $\epsilon_2(t)$, (v) the simulated and experimental PR responses.

experimental data shown in Figure 6 is also obtained along the entire interference oscillations. The agreement of the model with the experimental data in the several ways discussed above supports the efficiency of the ROSK model for describing the growth process and the observed optical response.

The parameters used for the minimization process in the determination of the unknown parameters in the model are presented in Table 2. The geometrical parameter $\gamma = 0.024$ was estimated in the minimization process for a two inch diameter circular substrate wafer.

The numerical solutions were calculated using programs written in MATLAB code. The stiff system of differential equations in the ROSK model was solved numerically by the built-in function “ode23s”, an adaptive mesh and low-order Runge-Kutta method [15]. The least squares optimization problem was solved using a Nelder-Mead [16, 17, 18] algorithm.

molar volumes (cm^3/mol)		sticking coefficients	effective SRL thickness
$V_{TBP} = 128.57$	$V_1 = 17.02$	$\beta_{TBP} = 0.15$	$\alpha_{SRL} = 0.75$
$V_{TEG} = 148.36$	$V_2 = 13.00$	$\beta_{TEG} = 1.0$	
$V_{TMI} = 101.99$	$V_3 = 11.80$	$\beta_{TMI} = 1.0$	
$V_{GaP} = 12.21$	$V_5 = 13.00$		
$V_{InP} = 15.22$	$V_6 = 15.71$		

Table 2: Constants used in the calculations of the model

We estimated the following parameters in the four layer stack model by averaging the results of independent best fits of the experimental data sets corresponding to different TMI:TEG flow ratios: the rate constants $k_1 = 3.57 \text{ s}^{-1}$, $k_{dTEG} = 0.60 \text{ s}^{-1}$, $k_2 = 1.87 \text{ s}^{-1}$, $k_3 = 0.05 \text{ s}^{-1}$, $k_{GaP} = 1.86 \text{ s}^{-1}$, $k_{dTMI} = 0.52 \text{ s}^{-1}$, $k_5 = 0.62 \text{ s}^{-1}$, $k_6 = 0.52 \text{ s}^{-1}$, and $k_{InP} = 1.58 \text{ s}^{-1}$; and the optical responses $F_1 = 12.77 - 0.05i$, $F_2 = 13.09 - 0.92i$, $F_3 = 7.96 - 4.66i$, $F_5 = 11.43 - 1.11i$, and $F_6 = 4.52 - 9.93i$. The averages of the SRL dielectric function for these parameters are given in Table 3 for each TMI:TEG flow ratio. Figure 7 shows the film composition from the model plotted against experimental data as a function of the TMI:TEG flow ratios.

TMI:TEG flow ratio	0.25	0.5	0.75	1.0	1.25
ϵ_2	12.32-1.51i	12.29-1.55i	12.39-1.38i	12.21-1.63i	11.99-1.90i

Table 3: Average values of the SRL dielectric function

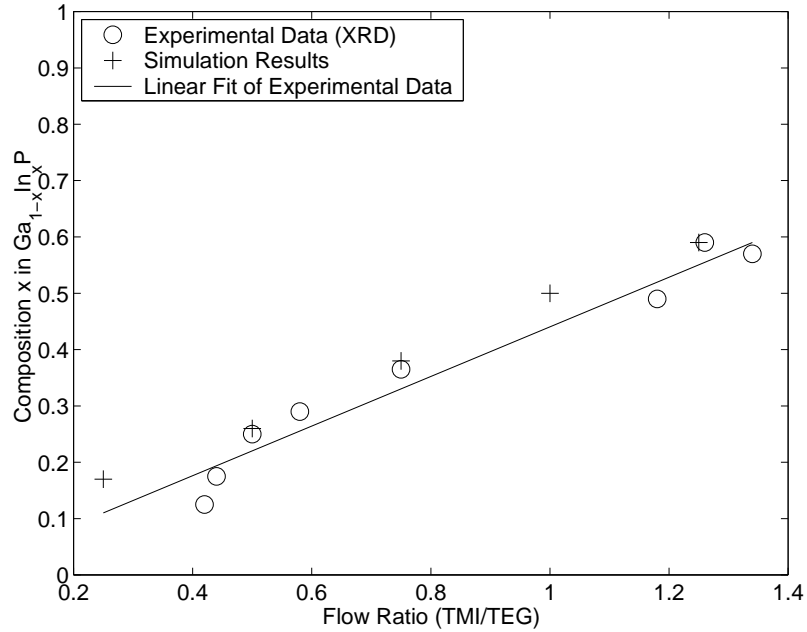


Figure 7: Film compositions for the simulations using various TMI:TEG flow ratios, as well as some experimental data points.

6. Conclusions

We extended our previous effort on utilizing a reduced order surface kinetics model using generalized reaction rate parameters for the growth of GaP [13] to describe the decomposition kinetics of the organometallic precursors TBP, TEG, and TMI used during the heteroepitaxial growth of $\text{Ga}_{1-x}\text{In}_x\text{P}$ on Si/GaP. A set of coupled differential equations was used to describe the surface reaction kinetics of our three precursor pulses and provided information about the dynamics of molar concentrations of precursor fragments stored in the surface reaction layer and their incorporation into the growing film. The model was validated and the unknown parameters involved were identified by fitting simulated PRS measurements from the model with several experimental data sets. The results demonstrate that a mathematical model can be effectively used to describe the film growth process. Current efforts are directed towards molecular specific optical process monitoring to validate the predicted surface reaction layer constituents and their concentrations as computed by the ROSK model.

7. Acknowledgements

The authors are grateful to Prof. Kelley, who is with the Department of Mathematics at North Carolina State University, for providing them with the code "nelder" implementing the Nelder-Mead algorithm. The authors also acknowledge support for this work by DOD-MURI Grant No. F49620-95-1-0447.

References

- [1] S. M. Bedair, B. T. McDermott, Y. Ide, N. H. Karam, H. Hashemi, M. A. Tischler, M. Timmons, J. C. L. Tarn, and N. El-Masry, "Recent Progress in Atomic Layer Epitaxy of III-V Compounds," *Journal of Crystal Growth*, Vol 93, pp. 182-189 (1988).
- [2] C. R. Abernathy, "Growth of III-V Materials by Metalorganic Molecular-Beam Epitaxy," *Journal of Vacuum Science and Technology A*, Vol 11, pp. 869-875 (1993).
- [3] D. E. Aspnes and N. Dietz, "Optical Approaches for Controlling Epitaxial Growth," *Applied Surface Science*, Vol 132, pp. 367-376 (1998).
- [4] N. Dietz, V. Woods, K. Ito, and I. Lauko, "Real-Time Optical Control of $\text{Ga}_{1-x}\text{In}_x\text{P}$ Film Growth by p -Polarized Reflectance," *Journal of Vacuum Science and Technology A*, Vol. 17, pp. 1300-1306 (1999).
- [5] N. Dietz and K. J. Bachmann, "Real-Time Monitoring of Epitaxial Processes by Parallel-Polarized Reflectance Spectroscopy," *MRS Bulletin*, Vol 20, pp. 49-55 (1995).
- [6] N. Dietz and K. J. Bachmann, " p -Polarized Reflectance Spectroscopy: A Highly Sensitive Real-Time Monitoring Technique to Study Surface Kinetics Under Steady State Epitaxial Deposition Conditions," *Vacuum*, Vol 47, pp. 133-140 (1996).
- [7] N. Dietz, N. Sukidi, C. Harris, and K. J. Bachmann, "Real-Time Monitoring of Surface Processes by p -Polarized Reflectance," *Journal of Vacuum Science and Technology A*, Vol 15, pp. 807-815 (1997).
- [8] N. Dietz and K. Ito, "Real-Time Optical Characterization of GaP Heterostructures by p -Polarized Reflectance," *Thin Solid Films*, Vol 313, pp. 614-619 (1998).
- [9] O. S. Heavens, *Optical Properties of Thin Solid Films*, London: Butterworths, 1955.
- [10] K. J. Bachmann, N. Sukidi, C. Hopfner, C. Harris, N. Dietz, H. T. Tran, S. Beeler, K. Ito, and H. T. Banks, "Real-Time Monitoring of Steady-State Pulsed Chemical Beam Epitaxy by p -Polarized Reflectance," *Journal of Crystal Growth*, Vol 183, pp. 323-337 (1998).
- [11] A. J. Murrell, A. T. S. Wee, D. H. Fairbrother, N. K. Singh, J. S. Foord, G. J. Davies, and D. A. Andrews, "Surface Studies of the Thermal-Decomposition of Triethylgallium on GaAs(100)," *Journal of Crystal Growth*, Vol 105, pp. 199-202 (1990).
- [12] K. J. Bachman, U. Rossow, and N. Dietz, "Real-Time Monitoring of Heteroepitaxial Growth Processes on the Silicon(001) Surface by p -Polarized Reflectance Spectroscopy," *Materials Science and Engineering B*, Vol 35, pp. 472-478 (1995).
- [13] S. Beeler, H. T. Tran, and N. Dietz, "Representation of GaP Formation by a Reduced Order Surface Kinetics Model Using p -Polarized Reflectance Measurements," *Journal of Applied Physics*, Vol 86, pp. 674-682 (1999).

- [14] G. Burns, *Solid State Physics*, p. 461, Orlando: Academic, 1985.
- [15] J. Stoer and R. Bulirsch, *Introduction to Numerical Analysis*, Second Edition, New York: Springer-Verlag, 1993.
- [16] D. M. Bortz and C. T. Kelley, "The Simplex Gradient and Noisy Optimization Problems," in *Computational Methods for Optimal Design and Control*, edited by J. T. Borggaard, J. Burns, E. Cliff, and S. Schreck, pp. 77-90, Boston: Birkhauser, 1998.
- [17] C. T. Kelley, "Detection and Remediation of Stagnation in the Nelder-Mead Algorithm Using a Sufficient Decrease Condition," *SIAM Journal on Optimization*, Vol 10, pp. 43-55 (1999).
- [18] C. T. Kelley, *Iterative Methods for Optimization*, Philadelphia: SIAM (ISBN 0-89871-433-8), 1999.